



1 **North China Plain as a hot spot of ozone pollution exacerbated**
2 **by extreme high temperatures**

3

4 Pinya Wang¹, Yang Yang^{1*}, Huimin Li¹, Lei Chen¹, Ruijun Dang², Daokai Xue³, Baojie Li¹,

5 Jianping Tang³, L. Ruby Leung⁴, Hong Liao¹

6 ¹Jiangsu Key Laboratory of Atmospheric Environment Monitoring and Pollution

7 Control, Jiangsu Collaborative Innovation Center of Atmospheric Environment and

8 Equipment Technology, School of Environmental Science and Engineering, Nanjing

9 University of Information Science and Technology, Nanjing, Jiangsu, China

10 ²School of Engineering and Applied Science, Harvard University, Cambridge, MA, USA

11 ³School of Atmospheric Sciences, Nanjing University, Nanjing, Jiangsu, China

12 ⁴Atmospheric Sciences and Global Change Division, Pacific Northwest National Laboratory,

13 Richland, Washington, USA

14

15 Correspondence to: Y. Yang, yang.yang@nuist.edu.cn

16



17 **Abstract**

18 A large population in China has been increasingly exposed to both severe ozone (O₃) pollution
19 and extreme heat under global warming. Here, the spatiotemporal characteristics of coupled
20 extremes in surface O₃ and heat (OPCs) over China are investigated using surface observations, a
21 process-based chemical transport model (GEOS-Chem), and multi-model simulations from Phase
22 6 of the Coupled Model Intercomparison Project (CMIP6). North China Plain (NCP, 37-41°N; 114-
23 120°E) is identified as a hot spot of OPCs, where more than half of the O₃ pollution days are
24 accompanied by high temperature extremes. OPCs over NCP exceed 40 days during 2014-2019,
25 exhibiting an increasing trend. Both O₃ concentrations and temperatures are elevated during OPCs
26 compared to O₃ pollution days occurring individually (OPIs). Therefore, OPCs impose more severe
27 health impacts to human than OPIs, but the stronger health effects are mainly driven by the higher
28 temperatures. GEOS-Chem simulations further reveal that enhanced chemical production resulting
29 from hot and stable atmospheric condition under anomalous weather pattern primarily contributes
30 to the exacerbated O₃ levels during OPCs. In the future, CMIP6 projections suggest increased
31 occurrences of OPCs over NCP in the middle of this century, but by the end of this century, OPCs
32 may decrease or increase depending on the pollutant emission scenarios. However, for all future
33 scenarios, extreme high temperature will play an increasingly important role in modulating O₃
34 pollution in a warming climate.

35

36

37



38 1. Introduction

39 With the rapid economic development, car ownership and fossil fuel consumption, China has
40 been struck by severe air pollution in the recent decades (Lu et al., 2018). Research and air quality
41 controls have been prioritized to tackle the problem of particulate matter, e.g., PM_{2.5} (T Wang et al.,
42 2017). Since the implementation of China's Action Plan on the Prevention and Control of Air
43 Pollution Plan in 2013, anthropogenic emissions of many air pollutants and their precursor gases,
44 including sulfur dioxide (SO₂), nitrogen oxides (NO_x), carbon monoxide (CO), black carbon (BC)
45 and organic carbon (OC), decreased by 21-59% between 2013 and 2017, despite a 11% increase in
46 anthropogenic emissions of non-methane volatile organic compounds (NMVOCs) (Zheng et al.,
47 2018). Correspondingly, the annual average PM_{2.5} concentrations decreased from 72 µg/m³ to 47
48 µg/m³ in 74 major cities in China (Huang et al., 2018). In contrast, ozone (O₃) concentrations in
49 China show an apparent increasing trend during 2013-2017, with the annual average O₃
50 concentrations in 74 key cities increasing from 140 µg/m³ to 160 µg/m³ (Huang et al., 2018). During
51 the warm season (April-September) of the same period, the daily maximum 8-hour average O₃
52 concentration (MDA8 O₃) increased at a rate of 3% per year, far exceeding the rates in many other
53 countries, such as Japan, Korea, and Europe (Lu et al., 2018). Long-term exposure to high O₃
54 concentrations can seriously damage human health, agriculture, buildings, and ecology (Sharma et
55 al., 2017, Yue et al., 2017). Therefore, the rising O₃ concentration in recent years has caused great
56 public concerns in China.

57 With global warming, extreme high temperatures and heat events have become natural hazards
58 in China in the recent decades, with substantial effect on socioeconomics, ecosystems and human
59 health (Lau and Nath, 2014, Meehl and Tebaldi, 2004). For instance, southern China was hit by a



60 widespread heat wave with a record-breaking maximum temperature of 43.2°C during summer 2003.
61 The extreme heat event lasted for more than 40 days and caused heightened levels of human
62 mortality (Tan et al., 2007, P Wang et al., 2017a). Such disastrous high temperatures have become
63 more frequent in China, as recorded subsequently in the summers of 2006, 2010, and 2013 (W Wang
64 et al., 2016). Recent studies found that extreme high temperatures and heat events have intensified
65 in the past 60 years and are expected to become more frequent and severe in the coming decades (P
66 Wang et al., 2019a; 2017b).

67 Extreme high temperatures are conducive to O₃ pollution. Specifically, high temperatures can
68 increase the production rate of surface O₃ in the presence of abundant O₃ precursors (Camalier et
69 al., 2007, Lu et al., 2019a). As O₃ concentration increases nonlinearly with temperature, extreme
70 high temperatures have disproportionate impacts on O₃ (Lin et al., 2020). Therefore, O₃ pollution
71 often co-occurs with extreme heat (Schnell and Prather, 2017). Besides the direct impacts of air
72 temperatures on O₃ production, the co-occurrence of extreme heat and O₃ pollution arise from their
73 shared underlying drivers, i.e., persistent high pressure, strong solar radiation, low humidity and
74 weak wind speeds (P Wang et al., 2017a; 2017b; Perkins, 2015). Hence despite reductions in
75 anthropogenic emissions of O₃ precursors in the U.S., Europe and China, high O₃ episodes will
76 likely continue in the future due to increasing heat waves under climate warming (Zhang et al.,
77 2018).

78 The coupled extremes in heat and O₃ pollution lead to higher mortality rates than O₃ pollution
79 or hot extreme acting alone (Krug et al., 2019). While the impacts of extreme high temperatures on
80 O₃ pollution have been investigated using case studies in China (Ma et al., 2019; Pu et al., 2017),
81 there is a gap in understanding the spatiotemporal characteristics and underlying mechanisms of



82 coupled extremes in high temperatures and O₃ pollution due to a lack of systematic analyses.
83 Although extreme high temperatures are expected to be more frequent and intense in the future with
84 accelerated warming, surface O₃ concentrations are expected to decrease because of curtailment in
85 O₃ precursor emissions. Therefore, considerable uncertainties exist in the future changes of coupled
86 extremes in heat and O₃.

87 In this study, based on the available surface O₃ concentrations and air temperatures
88 observations during 2014-2019, we investigate the spatiotemporal characteristics of co-occurrences
89 of extremes in air temperatures and surface O₃ in China, highlighting North China Plain (NCP,
90 defined here as 37-41°N; 114 -120°E, see Fig.1) as a hot spot which has already suffered from the
91 most severe O₃ pollution in recent years (K Li et al., 2019). The underlying mechanisms governing
92 the coupled extreme are examined using the global chemical transport model GEOS-Chem. The
93 associated health burden during the coupled extreme days is also discussed. In addition, future
94 projections of the coupled extremes in the warming climate are explored based on the latest multi-
95 model simulations from Phase 6 of the Coupled Model Intercomparison Project (CMIP6).

96 **2. Data and Method**

97 **2.1 Observed O₃ concentration and reanalysis data**

98 Hourly O₃ concentrations for 2014–2019 are obtained from China National Environmental
99 Monitoring Centre (CNEMC). The network covered 944 sites in 2014 that grew to about 1600 sites
100 in 2019. The daily maximum air temperatures (T_{max}) for more than 2000 observation sites during
101 the same period are provided by the National Meteorological Information Center of the China
102 Meteorological Administration (CMA). The dataset has been quality-controlled and homogenized
103 (Q Li et al., 2004) and widely used in previous works (P Wang et al., 2019b). Here in this study, we



104 focus on the extreme high temperatures and surface O₃ of warm season during May to September.
105 To unify the spatial resolutions of Tmax and O₃ concentration, the two observational datasets are
106 mapped to 1° × 1° grid boxes, and the values in each box represent the averaged observations within
107 that box. The spatial distributions of averaged daily Tmax and MDA8 O₃ over May-September
108 during 2014-2019 are shown in Figure S1.

109 Meteorological conditions during extremes of O₃ and high temperatures are calculated using
110 variables derived from the new Japanese 55-year Reanalysis (JRA-55) at 1.25° × 1.25° resolution
111 (Ebita et al., 2011), including geopotential height (HGT), winds, relative humidity (RH), 2m air
112 temperature (T2m), surface soil moisture (SM), downward solar radiation flux (DSR) and sensible
113 heat flux (SH). Following Gong and Liao (2019), daily time series of a meteorological parameter x
114 at a specific model grid cell over the months of May to September in the years 2014–2019 is
115 standardized by

$$116 \quad [x_i] = \frac{x_i - \frac{\sum_{i=1}^n x_i}{n}}{s}, \quad (1)$$

117 where x_i indicates the parameter x on day i, n is the total number of days during May to
118 September for 2014-2019, s indicates the standard deviation of the daily time series and $[x_i]$ is the
119 standardized anomaly for parameter x on day i.

120 2.2 GEOS-Chem model

121 To explore the physical and chemical mechanisms related to the O₃ extremes, the 3-D global
122 chemical transport model (GEOS-Chem, version 12.9.3) is utilized to simulate O₃ concentrations
123 during May-September for 2014-2017, driven by assimilated meteorological data of Version 2 of
124 Modern Era Retrospective-analysis for Research and Application (MERRA-2) (Gelaro et al., 2017).



125 The simulations are performed at a horizontal resolution of 2° latitude \times 2.5° longitude with 47
126 vertical levels. The anthropogenic emissions of O_3 precursor gases including CO, NO_x and VOCs
127 in China are obtained from the MEIC emission inventory (<http://meicmodel.org/>), which includes
128 emissions from industry, power, residential and transportation sectors. Lacking anthropogenic
129 emissions for 2018-2019, simulations are conducted for 2014-2017 by GEOS-Chem and we use
130 observations during 2014-2017 to validate the model results.

131 **2.3 CMIP6 data**

132 We use O_3 and Tmax outputs from future projections of Scenario Model Intercomparison
133 Project (ScenarioMIP) in the CMIP6 archive to determine how the coupled extremes will change in
134 a warmer climate. ScenarioMIP is the primary activity within CMIP6 that provides multi-model
135 climate projections driven by different scenarios of future emissions and land use changes (O'Neill
136 et al., 2016), produced based on the Shared Socioeconomic Pathways (SSPs) combining
137 socioeconomic developments and the feedback of global climate changes (Z Li et al., 2020). More
138 details about the SSP scenarios can be found in O'Neill et al. (2016).

139 Currently, four SSP scenarios in ScenarioMIP simulations provide hourly O_3 concentration
140 and daily Tmax from the present day to the end of the 21st century (2015 to 2100), i.e., SSP1-2.6,
141 SSP2-4.5, SSP3-7.0 and SSP5-8.5 (combination of low, intermediate, relatively high and high
142 societal vulnerabilities and forcing levels, respectively). Among the four SSPs, SSP3-7.0 and SSP2-
143 4.5 have the weakest and medium air pollution controls pathways, respectively, while strong air
144 pollution controls are assumed in SSP1-2.6 and SSP5-8.5 (Gidden et al., 2019). Five global climate
145 models (GCMs), MOHC.UKESM1-0-LL, CESM2-WACCM, GFDL-ESM4, MPI-ESM-1-2-HAM
146 and EC-Earth3-AerChem from ScenarioMIP under CMIP6 that provide both hourly O_3 and daily



147 Tmax are adopted in this work. The horizontal resolutions and institutions of the five GCMs are
148 listed in Table S1. Note that the numbers of available models vary across different scenarios (see
149 Table S2 for details). The results from the five GCMs are regridded to the observation boxes using
150 linear interpolation to facilitate spatial comparison. In this study, 2015-2019 is regarded as the
151 historical period and the overall performance of the CMIP6 simulations in reproducing the
152 occurrences of coupled extremes is evaluated against the observations during 2015-2019. For the
153 projection of coupled extremes, we focus on two periods of 2046-2050 and 2096-2100 in the mid
154 and end of the 20th century, respectively, under different SSPs.

155 **2.4 Identification of extremes in O₃ and temperature**

156 Following Schnell and Prather (2017), in this study, we use the local-specific thresholds for
157 each grid to identify the extreme cases of surface air temperatures and O₃ concentrations,
158 specifically, the 90th percentile of daily Tmax and daily MDA8 O₃ from May to September for
159 2014-2019. To characterize the co-occurrences of extremes in high temperatures and surface O₃ and
160 investigate the impacts of extreme high temperatures on O₃ pollution, the following extremes are
161 defined:

- 162 • Total O₃ pollution days (OPs): All days when daily MDA8 O₃ is above its threshold.
- 163 • Individual O₃ pollution days (OPIs): Days when MDA8 O₃ is above its threshold while Tmax
164 is lower than its threshold.
- 165 • Coupled extreme days (OPCs): Days when both daily Tmax and daily MDA8 O₃ exceed their
166 corresponding thresholds.

167 We use a co-occurrence frequency ratio (CF) in percent to characterize the dependence of extreme
168 high O₃ levels on extreme high temperatures. CF is defined as the ratio of the frequency of OPCs



169 (days) to the frequency of OPs (days). Thus, a higher CF value indicates a higher dependence of O₃
170 pollution on extreme high temperatures:

$$171 \quad CF = \text{OPCs/OPs} \times 100\%, \quad (2)$$

172 2.5 Health impact of coupled extremes

173 In this study, we apply the mortality ratio (MR) to describe the combined human health impacts
174 from O₃ and temperature levels during OPCs, following Lee et al. (2017). The MR ratio
175 characterizes the differences in health burden related to O₃ and temperature levels between OPCs
176 and OPIs, and MR is defined as below:

$$177 \quad MR = \frac{\text{Daily Mortality during OPCs}}{\text{Daily Mortality during OPIs}}$$
$$178 \quad = \frac{\frac{\sum_i RR_{\text{ozone},i}}{m}}{\frac{\sum_j RR_{\text{ozone},j}}{n}} \cdot \frac{\frac{\sum_i RR_{\text{temperature},i}}{m}}{\frac{\sum_j RR_{\text{temperature},j}}{n}}, \quad (3)$$

$$179 \quad MR_{\text{ozone}} = \frac{\frac{\sum_i RR_{\text{ozone},i}}{m}}{\frac{\sum_j RR_{\text{ozone},j}}{n}}, \quad (4)$$

$$180 \quad MR_{\text{temperature}} = \frac{\frac{\sum_i RR_{\text{temperature},i}}{m}}{\frac{\sum_j RR_{\text{temperature},j}}{n}}, \quad (5)$$

$$181 \quad RR_{\text{ozone}} = \exp(\beta_1(C - C_0)), \quad (6)$$

$$182 \quad RR_{\text{temperature}} = \exp(\beta_2(T - T_0)), \quad (7)$$

183 Here, $RR_{\text{ozone},i}$ ($RR_{\text{ozone},j}$) and $RR_{\text{temperature},i}$ ($RR_{\text{temperature},j}$) are the relative risks due to O₃
184 concentration and temperature exceeding the threshold of C_0 and T_0 , respectively, on a coupled
185 extreme day i (an individual O₃ pollution day j); m is the total days of coupled extremes and n is the
186 total days of individual O₃ pollution day. MR_{ozone} ($MR_{\text{temperature}}$) is the mortality ratio attributed to



187 O₃ concentration (temperature) changes, while MR is the combined effects from both O₃ and
188 temperature changes.

189 For the calculation of RR_{ozone} in Eq. 6, C_0 is the minimum O₃ concentration below which O₃
190 has no health impacts. C_0 is set to zero here as previous work found no significant threshold for the
191 O₃ related mortality (K Chen et al., 2017). β_1 is the concentration response factor corresponding to
192 a 0.24% [95% confidence interval: 0.13%, 0.35%] increase in daily mortality per 10 $\mu\text{g}/\text{m}^3$ increase
193 in MDA8 O₃ (Yin et al., 2017). Following Huang et al. (2018) in calculating $RR_{\text{temperature}}$ in 66
194 Chinese communities, β_2 indicates a 1.09% (95% confidence interval: 0.72% to 1.46%) excess
195 mortality per 1°C increase in temperature above T_0 , which is the minimum mortality temperature
196 set as 26°C in this study (C Wang et al., 2014).

197 **3. Results**

198 **3.1 Spatial and temporal patterns of coupled extremes**

199 The spatial patterns of OPCs and their ratio to the total O₃ pollutions days (CF values) during
200 May-September for the recent 6 years (2014-2019) highly resemble each other (Figure 1), with the
201 highest values located over NCP which has suffered the most severe O₃ pollution in recent years
202 (Fig.S1a). The highest OPCs exceed 40 days over NCP and the corresponding CF is more than 56%
203 (Fig. 1). That means, the coupled extreme days account for more than half of the total O₃ pollution
204 days, indicating a strong dependence of O₃ pollution on extreme high temperatures over NCP. It has
205 been suggested that the dependence of O₃ concentration on high temperature increases with the O₃
206 levels (Lin et al., 2020). However, coupled extremes occur much less frequently over the Yangtze
207 River Delta (YRD, 30-33°N, 118-122°E) compared to NCP, and the regional averaged CF in YRD
208 is below 20%, even though MDA O₃ level and temperature in YRD are both as high as those in



209 NCP (Fig. S1). The distinctive relationships between extreme high temperature and O₃
210 concentration over NCP and YRD are driven by their different climatology during warm season.
211 Southern China receives substantial monsoon rainfall during summer, accompanied by increased
212 relative humidity (RH) and reduced radiation (Zhou and Yu, 2005), which can suppress surface O₃
213 levels (Han et al., 2020). Delineating the local daily maximum air temperatures (T_{max}) and RH of
214 all O₃ pollution days over NCP and YRD (Figure S2), OPCs occur more frequently over NCP than
215 over YRD, and a higher fraction of the O₃ pollution days over NCP co-occur with extreme high
216 temperatures and low-to-moderate RH (Fig. S2a). Humid environment dampens the occurrence of
217 O₃ pollution over YRD and extreme O₃ pollution mostly occurs on days with relatively low RH
218 when air temperatures are moderate (Fig. S2b), which explains the lower OPCs and CF in YRD
219 compared to NCP. Therefore, we focus on the coupled extremes over NCP.

220 Daily variations of the occurrence of OPIs and OPCs over NCP during 2014–2019 are shown
221 in Figure 2. O₃ pollution days have appeared since 2015 but coupled extremes OPCs have only been
222 observed since 2017, mostly during May–July (Fig. 2a). The abrupt increase in the occurrence of
223 coupled extremes in 2017 is consistent with the significant increasing trends of both MDA8 O₃ and
224 T_{max} (95% confidence level) over NCP in recent years (Fig. 2b). The strong increasing trend of
225 MDA8 O₃ and temperature. The strong increasing trends of MDA8 O₃ and air temperatures are
226 consistent with previous results (K Li et al., 2019; 2020). As addressed previously (K Li et al.,
227 2020), the temperature trends during 2014–2019 reflect interannual climate variability rather than a
228 long-term warming trend. Notably, daily MDA8 O₃ exhibits increasing sensitivity to T_{max} from
229 2014 to 2019 (Fig. 2c), supporting the increase in OPCs during the same time period. Note that the
230 linear regression slopes between daily MDA8 O₃ and T_{max} are not strictly monotonic increasing.



231 For example, the slopes are 3.96 ppbv/°C, 3.43 ppbv/°C and 4.56 ppbv/°C in 2017, 2018, and 2019
232 (Fig. 2c). In fact, the yearly occurrences of OPCs are 15, 13, 18 days in 2017, 2018, 2019, consistent
233 with ozone and temperature relationship. Thus, what we emphasize here is the overall increasing
234 OPCs during 2014 to 2019 with an abrupt increase of OPCs since 2017. The contrasting MDA8 O₃
235 and Tmax associated with OPCs and OPIs over NCP are evident in Fig. 3. Both O₃ levels and air
236 temperatures are higher during OPCs than during OPIs over NCP region (Fig.3a&3b), with the
237 regional mean anomalies of Tmax and MDA8 O₃ during OPCs reaching 3.36°C and 5.49 ppbv,
238 respectively, compared to those during OPIs. A north-south contrast in the MDA8 O₃ and Tmax
239 difference between OPCs and OPIs is evident (Fig. 3b), suggesting that contrasting environments
240 north and south of the Yangtze River during the summer monsoon may play a key role in the
241 dependence of O₃ pollution on extreme Tmax in China.

242 **3.2 Weather patterns and ozone processes during coupled extremes**

243 Figure 4 shows the composites of normalized anomalies (see Sec.2) of meteorological fields
244 during coupled extreme days over NCP for 2014-2019. During OPCs, anomalous high pressure and
245 anticyclonic circulation dominate NCP and the surrounding region north of the Yangtze River in
246 the mid-troposphere (500hPa), with anomalous easterlies prevailing over NCP (Fig.4a). Associated
247 with the anomalous high-pressure system is clear sky with enhanced downward solar radiation
248 (DSR) at the surface (Fig.4c), leading to hotter near surface temperature (Fig.4b), reduced RH and
249 soil moisture (Fig. 4d&4e), and enhanced surface sensible heat flux (Fig.4f) that further intensifies
250 the temperatures (Fig. 4b). These anomalous conditions are all stronger during OPCs than OPIs over
251 NCP (Fig. S3) and more conducive to O₃ pollutions (Lu et al., 2019b). Among the meteorological
252 factors, the intensification in surface temperatures is the strongest among different meteorological



253 variables with the highest magnitudes (Fig.S3b), supporting that air temperature is the most
254 influential meteorological variable of surface O₃ over NCP (K Li et al., 2019).

255 The impacts of weather patterns on surface O₃ level can be understood via changes in physical
256 and chemical processes, both sensitive to meteorology (L Chen et al., 2020). The contributions of
257 different chemical and physical processes to OPCs over NCP under the anomalous weather pattern
258 of Fig. 4 are quantified by GEOS-Chem simulations of O₃ during May to September of 2014–2017.
259 GEOS-Chem can reasonably capture the spatial pattern and magnitude of OPCs in observations
260 during 2014-2017 (Text S1 and Figure S4). Four processes affecting O₃ levels are considered,
261 including net chemical production, horizontal advection, vertical advection, and mixing (diffusion
262 plus dry deposition) and are listed in Table 1. For both OPIs and OPCs, chemical production
263 contributes the most to O₃ mass within the boundary layer. Compared to OPIs, the higher O₃ level
264 during OPCs (Fig. 3b) are contributed by stronger chemical production and mixing but vertical
265 advection and horizontal advection tend to reduce the O₃ concentrations, with enhanced chemical
266 production playing the dominant role. Therefore, we conclude that the hotter near surface
267 temperature induced by anomalous weather pattern and amplified by land-atmosphere feedbacks
268 during OPCs (Fig. 4) is the primary cause of the enhanced formation of O₃ and eventually a higher
269 surface O₃ level than during OPIs.

270 **3.3 Health impacts of coupled extremes**

271 As both surface O₃ and air temperatures are amplified during coupled relative to individual O₃
272 pollution days (Fig. 3), we investigate the potential influences of OPCs on human health. The
273 mortality ratios between OPCs and OPIs during May to September for each year of 2017-2019 are
274 illustrated in Figure 5 and attributed to air temperature and/or O₃ concentration changes



275 ($MR_{\text{Temperature}}$, MR_{Ozone} and MR , see Sec.2). It should be noted that coupled extreme days are only
276 observed since 2017. MR , MR_{Ozone} and $MR_{\text{Temperature}}$ are above 1.0 for all three years, indicating a
277 harsher environment for people to survive during OPCs. Importantly, $MR_{\text{Temperature}}$ is significantly
278 higher than MR_{Ozone} for all years of 2017-2019, suggesting that extreme high temperature caused
279 many more mortalities than extreme O_3 concentrations over NCP. The averaged MR_{Ozone} ,
280 $MR_{\text{Temperature}}$, and MR for 2017-2019 are 1.003, 1.037, and 1.040, respectively. Compared to the
281 individual O_3 pollution days OPs, daily mortality rate in NCP increases by 4.0% during coupled
282 extremes OPCs, the majority of which is attributed to the temperature increase, with less than one-
283 tenth contributed by the O_3 concentration increase. That is, coupled extremes amplify health impacts
284 compared to individual O_3 pollution days primarily because of the higher mortality risk associated
285 with elevated air temperatures.

286 **3.4 Projected coupled extremes in future climate**

287 As O_3 precursors (i.e., NO_x and $NMVOCs$) are expected to keep declining due to the continued
288 emission controls in China while extreme high temperatures will become more frequent and intense
289 under global warming, uncertainties exist in the projection of the co-occurrences of extremes in
290 high temperatures and O_3 pollution. Here, we investigate the projections of OPCs and CF values
291 based on CMIP6 simulations under SSP1-2.6, SSP2-4.5, SSP3-7.0 and SSP5-8.5. OPCs in the
292 simulations are identified in the same way as for the observations (see Text S2 and Fig S5 for details).
293 We focus on the historical period of 2015-2019 (referred to as 2019) and the projected periods of
294 2046-2050 (referred to as 2050) and 2096-2100 (referred to as 2100) by the mid and end of the
295 century. Note that OPCs during the projected periods are identified based on the historical
296 thresholds for extreme O_3 level and high temperatures. The multi-model ensemble means can



297 reasonably capture the observed spatial pattern of coupled extremes and their magnitudes over NCP
298 during 2015-2019 (Fig. S5).

299 The averaged OPCs over NCP under each SSP increase from the historical period to the mid-
300 century (Fig. 6a), with a maximum increase under SSP5-8.5 (spatial distribution shown in Fig. S6).
301 From the mid-century to the end-century, OPCs decrease under SSP1-2.6, SSP2-4.5 and SSP5-8.5,
302 but OPCs by 2100 obviously surpass that in 2050 under SSP3-7.0, with an average increase from
303 46 days to 196 days (spatial patterns in Fig.S6e&S6f). Due to the weak air pollution control under
304 SSP3-7.0 (Turnock et al., 2020), MDA8 O₃ in 2100 under this scenario is highest among the four
305 SSPs (Fig. S8). In contrast, OPCs are substantially reduced to below 5 days by 2100 under SSP1-
306 2.6 and SSP2-4.5, highlighting the benefit of strong actions in mitigating climate and reducing air
307 pollutant emissions. In the future by 2050 and 2100, NCP will still be the most vulnerable region in
308 China to the coupled extreme (Figure S6), while most other areas will be much less threatened by
309 the coupled extremes by the end of the century under SSP1-2.6, SSP2-4.5 and SSP5-8.5 (Fig. S6b,
310 S6d, and S6h).

311 Unlike OPCs, CF over NCP obviously increases by the 2050 and 2100 compared to 2019 under
312 all four SSPs (Fig. 6b). The projected increases of CF over NCP indicate the higher dependence of
313 O₃ pollution on extreme high temperatures in the future, consistent with the increased sensitivity of
314 MDA8 O₃ to T_{max} at higher T_{max} in historical period (Fig. 2c). Spatially, the NCP region will still
315 see the highest CF values in the future, especially under SSP1-2.6, SSP2-4.5 and SSP5-8.5 (Fig.
316 S7). This means regardless of the economic pathways, extreme high temperature will play an
317 increasingly important role in modulating O₃ pollution in the warming climate. Therefore, besides



318 the management strategies on pollutants emission, global warming mitigations will undoubtedly
319 benefit O₃ pollution control, especially for regions facing severe air quality issues.

320 **4. Discussion and conclusions**

321 Climate change can impact local air quality. Higher temperatures associated with climate
322 change can lead to an increase in surface O₃, and high temperatures and surface O₃ are highly
323 temporally correlated over many regions (Porter et al., 2019). A large population in China has been
324 increasingly exposed to both severe O₃ pollution and extreme heat under global warming. With
325 combined surface observations of air temperature and O₃ concentration, process-based model
326 simulations and multi-model projections, this study firstly present a comprehensive analysis of the
327 co-occurrences of extreme high temperatures and O₃ pollution in China. It is highlighted that NCP
328 is a hot spot in China most threatened by the co-occurrence of extremes in heat and O₃ pollution.
329 The higher co-occurrence over NCP than other regions in China is linked to their distinctive
330 relations to meteorological variables, as temperature is the top meteorological factor directly leading
331 to O₃ pollution over NCP whereas relative humidity is the most influential variable for O₃ pollution
332 over southern China (Han et al., 2020).

333 The concurrent increasing trends in both surface O₃ and temperature over NCP in recent years
334 account for the increasing coupled extremes in surface O₃ and heat in recent years. Besides, it is
335 previously reported that the increasing trend of temperature is higher over northern China than
336 southern China (P Wang et al., 2017b; Qian et al., 2006). The increase in air temperature can
337 accelerate the O₃ production. Using a physically based model (GEOS-Chem), we have provided
338 support for the dominant role of higher temperatures associated with stable atmospheric
339 condition under favorable weather pattern in amplifying O₃ pollution through enhanced



340 chemical production during coupled extremes, compared to the individual ozone pollution days
341 not accompanied by extreme temperatures. In addition, the increases in surface O₃ over NCP are
342 much stronger than the other regions in recent years, which is also possibly linked to the stimulation
343 effect from enhanced hydroperoxyl radicals (HO₂) due to a reduction in aerosol sink resulting from
344 the decrease in PM_{2.5} during this period (K Li et al., 2019). Thus, the hot spot of co-occurrences of
345 extremes in heat and O₃ over NCP could be attributed to the co-effects of stronger increasing trends
346 of temperature and surface O₃ therein.

347 It is a prevalent concept that the coupled extremes pose greater health impacts or risks to human
348 than the simply summed impacts of the single extremes acting alone (Smith et al., 2014). It is
349 revealed here that both the O₃ concentration and air temperatures are elevated during the coupled
350 extremes than the individual O₃ pollution, leading to an even heavier health burden to human. And
351 this study underscores the elevated air temperatures during the coupled extremes as the major driver
352 for increased mortality rates, while the simultaneously elevated O₃ concentrations act as an
353 additional stressor. It should be noted that the algorithm we use to calculate MR, MR_{ozone} and
354 MR_{temperature} (see Sec.2) does not consider the possible amplification/inhibition effect of combining
355 O₃ and air temperature in affecting human health. Previous studies have claimed that O₃-related
356 mortality changes with different air temperature levels, with O₃-related mortality increasing with
357 higher temperatures, although several studies presented contrasting results or inconsistent
358 relationships for different regions (R Chen et al., 2014; Jhun et al., 2014; Ren et al., 2008). Therefore,
359 how the interactions between temperature and O₃ influence human health during coupled extremes
360 is still an open question that deserves future studies using more health-related data.



361 Currently, China has the highest emission of greenhouse gases, and the emission rates have
362 increased significantly since the 21st century (Friedlingstein et al., 2020). To prevent the dangerous
363 climate change impacts, the Chinese government has declared an ambitious goal by pledging to
364 peak emissions before 2030 and reaching carbon neutrality before 2060. With global warming, hot
365 extremes in China are projected to be more frequent, stronger, and longer lasting under global
366 warming, which may present challenges for O₃ pollution control of China. Based on ScenarioMIP
367 simulations from CMIP6, this study demonstrates that the coupled extremes over NCP are projected
368 to be more frequent in the middle of this century but their frequency decreases or increases by the
369 end of the century under strong or weak air pollution control scenarios, respectively. And with
370 higher sensitivity of O₃ concentration to temperatures at higher temperatures, O₃ extreme will
371 increasingly co-occur with extreme high temperatures over NCP as the climate warms, regardless
372 of the economic pathways. Thus, our results further reinforce the notion that determined actions are
373 vital to make our communities less vulnerable to climate change impacts already in progress. On
374 the other hand, tropospheric O₃ level are projected to be increasing in the near decades (Turnock et
375 al., 2020) (also see Fig. S8b). As the third important anthropogenic greenhouse gas after CO₂ and
376 CH₄, tropospheric O₃ radiative forcing over the industrial era is $0.4 \pm 0.2 \text{ W m}^{-2}$ (Myhre et al.,
377 2014). Higher tropospheric O₃ level can cause temperature changes by altering the energy balance
378 between the atmosphere and the Earth (Dang and Liao, 2019), which may feedback on the air quality.
379 Thus, potential co-benefits may be gained through O₃ pollution control and climate change
380 managements, in suppressing the occurrences of coupled extremes and tackling their consequences
381 to air quality, human health, and climate.

382



383 **Data availability**

384 Hourly O₃ concentrations are obtained from the public website of the China National Environmental
385 Monitoring Centre (<http://www.cnemc.cn/en/>). Daily maximum air temperature is provided by the
386 National Meteorological Information Center of the China Meteorological Administration (CMA,
387 <http://data.cma.cn/en/>). Reanalysis datasets are derived from the new Japanese 55-year Reanalysis
388 (<https://rda.ucar.edu/datasets/ds628.0/>). Multi-model projections are from Scenario Model
389 Intercomparison Project in Phase 6 of the Coupled Model Intercomparison Project ([https://esgf-
390 node.llnl.gov/search/cmip6/](https://esgf-
390 node.llnl.gov/search/cmip6/)). The GEOS-Chem model is available at
391 <http://acmg.seas.harvard.edu/geos/>.

392 **Author contributions**

393 P. Wang performed the analyses and wrote the initial draft. Y. Yang conceived and supervised the
394 study. H. Li performed the GEOS-Chem simulations. Y. Yang and L.R. Leung reviewed and edited
395 the initial draft. All the authors discussed the results and contributed to the final manuscript.

396 **Competing interests**

397 The authors declare that they have no competing interest.

398 **Acknowledgements**

399 This work is supported by the National Key Research and Development Program of China (grant
400 2020YFA0607803 and 2019YFA0606800). LRL was supported by the U.S. Department of Energy
401 Office of Science Biological and Environmental Research through the Regional and Global



402 Modeling and Analysis program area. PNNL is operated for the Department of Energy by Battelle
403 Memorial Institute under contract DE-AC05-76RL01830.

404 **Financial support**

405 This study was supported by the National Key Research and Development Program of China (grant
406 2020YFA0607803 and 2019YFA0606800) and the U.S. Department of Energy Office of Science
407 Biological and Environmental Research through the Regional and Global Modeling and Analysis
408 program area.

409

410 **References**

411 Camalier, L., W. Cox, and P. Dolwick (2007), The effects of meteorology on ozone in urban areas
412 and their use in assessing ozone trends, *Atmospheric Environment*, 41(33), 7127-7137.

413 Chen, K., L. Zhou, X. Chen, J. Bi, and P. L. Kinney (2017), Acute effect of ozone exposure on
414 daily mortality in seven cities of Jiangsu Province, China: No clear evidence for threshold,
415 *Environ Res*, 155, 235-241.

416 Chen, L., J. Zhu, H. Liao, Y. Yang, and X. Yue (2020), Meteorological influences on PM2.5 and
417 O3 trends and associated health burden since China's clean air actions, *Sci Total Environ*,
418 744, 140837.



- 419 Chen, R., J. Cai, X. Meng, H. Kim, Y. Honda, Y. L. Guo, E. Samoli, X. Yang, and H. J. A. j. o. e.
420 Kan (2014), Ozone and daily mortality rate in 21 cities of East Asia: how does season modify
421 the association?, 180(7), 729-736.
- 422 Dang, R., and H. J. G. R. L. Liao (2019), Radiative Forcing and Health Impact of Aerosols and
423 Ozone in China as the Consequence of Clean Air Actions over 2012–2017, 46(21).
- 424 Ebita, A., et al. (2011), The Japanese 55-year Reanalysis "JRA-55": An Interim Report, Sola, 7,
425 149-152.
- 426 Friedlingstein, P., M. O'sullivan, M. W. Jones, R. M. Andrew, J. Hauck, A. Olsen, G. P. Peters,
427 W. Peters, J. Pongratz, and S. J. E. S. S. D. Sitch (2020), Global carbon budget 2020, 12(4),
428 3269-3340.
- 429 Gelaro, R., et al. (2017), The Modern-Era Retrospective Analysis for Research and Applications,
430 Version 2 (MERRA-2), J Clim, Volume 30(Iss 13), 5419-5454.
- 431 Gidden, M. J., K. Riahi, S. J. Smith, S. Fujimori, G. Luderer, E. Kriegler, D. P. v. Vuuren, M. v. d.
432 Berg, L. Feng, and D. J. G. m. d. Klein (2019), Global emissions pathways under different
433 socioeconomic scenarios for use in CMIP6: a dataset of harmonized emissions trajectories
434 through the end of the century, 12(4), 1443-1475.
- 435 Han, H., J. Liu, L. Shu, T. Wang, H. J. A. C. Yuan, and Physics (2020), Local and synoptic
436 meteorological influences on daily variability in summertime surface ozone in eastern China,
437 20(1), 203-222.



- 438 Huang, J., X. Pan, X. Guo, and G. J. T. L. P. H. Li (2018), Health impact of China's Air Pollution
439 Prevention and Control Action Plan: an analysis of national air quality monitoring and
440 mortality data, 2(7), e313-e323.
- 441 Jhun, I., N. Fann, A. Zanobetti, and B. J. E. i. Hubbell (2014), Effect modification of ozone-
442 related mortality risks by temperature in 97 US cities, 73, 128-134.
- 443 Krug, A., D. Fenner, A. Holtmann, and D. Scherer (2019), Occurrence and Coupling of Heat and
444 Ozone Events and Their Relation to Mortality Rates in Berlin, Germany, between 2000 and
445 2014, Atmosphere, 10(6).
- 446 Lau, N. C., and M. J. Nath (2014), Model Simulation and Projection of European Heat Waves in
447 Present-Day and Future Climates, Journal of Climate, 27(10), 3713-3730.
- 448 Lee, J. Y., S. H. Lee, S.-C. Hong, and H. Kim (2017), Projecting future summer mortality due to
449 ambient ozone concentration and temperature changes, Atmospheric Environment, 156, 88-
450 94.
- 451 Li, K., D. J. Jacob, H. Liao, L. Shen, Q. Zhang, and K. H. Bates (2019), Anthropogenic drivers of
452 2013-2017 trends in summer surface ozone in China, Proc Natl Acad Sci U S A, 116(2), 422-
453 427.
- 454 Li, K., D. J. Jacob, L. Shen, X. Lu, I. De Smedt, and H. Liao (2020), Increases in surface ozone
455 pollution in China from 2013 to 2019: anthropogenic and meteorological influences,
456 Atmospheric Chemistry and Physics, 20(19), 11423-11433, doi:10.5194/acp-20-11423-2020.



- 457 Li, Q., X. Liu, H. Zhang, P. Thomas C, and E. David R (2004), Detecting and adjusting temporal
458 inhomogeneity in Chinese mean surface air temperature data, *Advances in Atmospheric*
459 *Sciences*, 21(2), 260-268.
- 460 Li, Z., H. Tao, H. Hartmann, B. Su, Y. Wang, and T. Jiang (2020), Variation of Projected
461 Atmospheric Water Vapor in Central Asia Using Multi-Models from CMIP6, *Atmosphere*,
462 11(9).
- 463 Lin, M., L. W. Horowitz, Y. Xie, F. Paulot, and K. J. N. C. C. Pilegaard (2020), Vegetation
464 feedbacks during drought exacerbate ozone air pollution extremes in Europe, 10(5).
- 465 Lu, X., L. Zhang, and L. Shen (2019a), Meteorology and Climate Influences on Tropospheric
466 Ozone: a Review of Natural Sources, Chemistry, and Transport Patterns, *Current Pollution*
467 *Reports*, 5(4), 238-260.
- 468 Lu, X., J. Hong, L. Zhang, O. R. Cooper, M. G. Schultz, X. Xu, T. Wang, M. Gao, Y. Zhao, and
469 Y. Zhang (2018), Severe Surface Ozone Pollution in China: A Global Perspective,
470 *Environmental Science & Technology Letters*, 5(8), 487-494.
- 471 Lu, X., L. Zhang, Y. Chen, M. Zhou, B. Zheng, K. Li, Y. Liu, J. Lin, T.-M. Fu, and Q. Zhang
472 (2019b), Exploring 2016–2017 surface ozone pollution over China: source contributions and
473 meteorological influences, *Atmospheric Chemistry and Physics*, 19(12), 8339-8361.
- 474 Ma, M., et al. (2019), Substantial ozone enhancement over the North China Plain from increased
475 biogenic emissions due to heat waves and land cover in summer 2017, *Atmospheric*
476 *Chemistry and Physics*, 19(19), 12195-12207.



- 477 Meehl, G. A., and C. Tebaldi (2004), More intense, more frequent, and longer lasting heat waves
478 in the 21st century, *Science*, 305(5686), 994-997.
- 479 Myhre, G., D. Shindell, and J. Pongratz (2014), Anthropogenic and natural radiative forcing.
- 480 O'Neill, B. C., et al. (2016), The Scenario Model Intercomparison Project (ScenarioMIP) for
481 CMIP6, *Geoscientific Model Development*, 9(9), 3461-3482.
- 482 Perkins, S. E. (2015), A review on the scientific understanding of heatwaves—their measurement,
483 driving mechanisms, and changes at the global scale, *Atmospheric Research*, 164, 242-267.
- 484 Porter, W. C., C. L. J. A. C. Heald, and Physics (2019), The mechanisms and meteorological
485 drivers of the summertime ozone–temperature relationship, 19(21), 13367-13381.
- 486 Pu, X., T. J. Wang, X. Huang, D. Melas, P. Zanis, D. K. Papanastasiou, and A. Poupkou (2017),
487 Enhanced surface ozone during the heat wave of 2013 in Yangtze River Delta region, China,
488 *Sci Total Environ*, 603-604, 807-816.
- 489 Qian, W., A. J. M. Qin, and A. Physics (2006), Spatial-temporal characteristics of temperature
490 variation in China, 93(1), 1-16.
- 491 Ren, C., G. M. Williams, K. Mengersen, L. Morawska, and S. J. E. I. Tong (2008), Does
492 temperature modify short-term effects of ozone on total mortality in 60 large eastern US
493 communities?—An assessment using the NMMAPS data, 34(4), 451-458.



- 494 Schnell, J. L., and M. J. Prather (2017), Co-occurrence of extremes in surface ozone, particulate
495 matter, and temperature over eastern North America, *Proc Natl Acad Sci U S A*, 114(11),
496 2854-2859.
- 497 Sharma, S., P. Sharma, and M. Khare (2017), Photo-chemical transport modelling of tropospheric
498 ozone: A review, *Atmospheric Environment*, 159, 34-54.
- 499 Smith, K., A. Woodward, D. Campbell-Lendrum, D. Chadee, Y. Honda, Q. Liu, J. Olwoch, B.
500 Revich, R. Sauerborn, and C. Aranda (2014), Human health: impacts, adaptation, and co-
501 benefits, in *Climate Change 2014: impacts, adaptation, and vulnerability. Part A: global and*
502 *sectoral aspects. Contribution of Working Group II to the fifth assessment report of the*
503 *Intergovernmental Panel on Climate Change*, edited, pp. 709-754, Cambridge University
504 Press.
- 505 Tan, J., Y. Zheng, G. Song, L. S. Kalkstein, A. J. Kalkstein, and X. Tang (2007), Heat wave
506 impacts on mortality in Shanghai, 1998 and 2003, *International Journal of Biometeorology*,
507 51(3), 193-200.
- 508 Turnock, S. T., et al. (2020), Historical and future changes in air pollutants from CMIP6 models,
509 20(23), 14547-14579.
- 510 Wang, C., R. Chen, X. Kuang, X. Duan, and H. Kan (2014), Temperature and daily mortality in
511 Suzhou, China: a time series analysis, *Sci Total Environ*, 466-467, 985-990.
- 512 Wang, P., P. Hui, D. Xue, and J. J. C. D. Tang (2019a), Future projection of heat waves over
513 China under global warming within the CORDEX-EA- II project, 53(1-2), 957-973.



- 514 Wang, P., J. Tang, S. Wang, X. Dong, and J. Fang (2017a), Regional heatwaves in china: a cluster
515 analysis, *Climate Dynamics*, 1-17.
- 516 Wang, P., L. R. Leung, J. Lu, F. Song, and J. J. J. o. G. R. A. Tang (2019b), Extreme Wet - Bulb
517 Temperatures in China: The Significant Role of Moisture, *124(22)*, 11944-11960.
- 518 Wang, P., J. Tang, X. Sun, S. Wang, J. Wu, X. Dong, and J. Fang (2017b), Heatwaves in China:
519 definitions, leading patterns and connections to large - scale atmospheric circulation and
520 SSTs, *Journal of Geophysical Research Atmospheres*.
- 521 Wang, T., L. Xue, P. Brimblecombe, Y. F. Lam, L. Li, and L. Zhang (2017), Ozone pollution in
522 China: A review of concentrations, meteorological influences, chemical precursors, and
523 effects, *Science of The Total Environment*, 575, 1582-1596.
- 524 Wang, W., W. Zhou, X. Li, X. Wang, and D. Wang (2016), Synoptic-scale characteristics and
525 atmospheric controls of summer heat waves in China, *Climate Dynamics*, 46(9-10), 2923-
526 2941.
- 527 Yin, P., et al. (2017), Ambient Ozone Pollution and Daily Mortality: A Nationwide Study in 272
528 Chinese Cities, *Environ Health Perspect*, 125(11), 117006.
- 529 Yue, X., N. Unger, K. Harper, X. Xia, H. Liao, T. Zhu, J. Xiao, Z. Feng, and J. Li (2017), Ozone
530 and haze pollution weakens net primary productivity in China, *Atmospheric Chemistry and*
531 *Physics*, 17(9), 6073-6089.



532 Zhang, J., Y. Gao, K. Luo, L. R. Leung, Y. Zhang, K. Wang, and J. Fan (2018), Impacts of
533 compound extreme weather events on ozone in the present and future, Atmospheric
534 Chemistry and Physics, 18(13), 9861-9877.

535 Zheng, B., et al. (2018), Trends in China's anthropogenic emissions since 2010 as the consequence
536 of clean air actions, 18(19), 14095-14111.

537 Zhou, T. J., and R. C. Yu (2005), Atmospheric water vapor transport associated with typical
538 anomalous summer rainfall patterns in China, Journal of Geophysical Research Atmospheres,
539 110(8), 211-211.

540

541

542

543

544

545

546

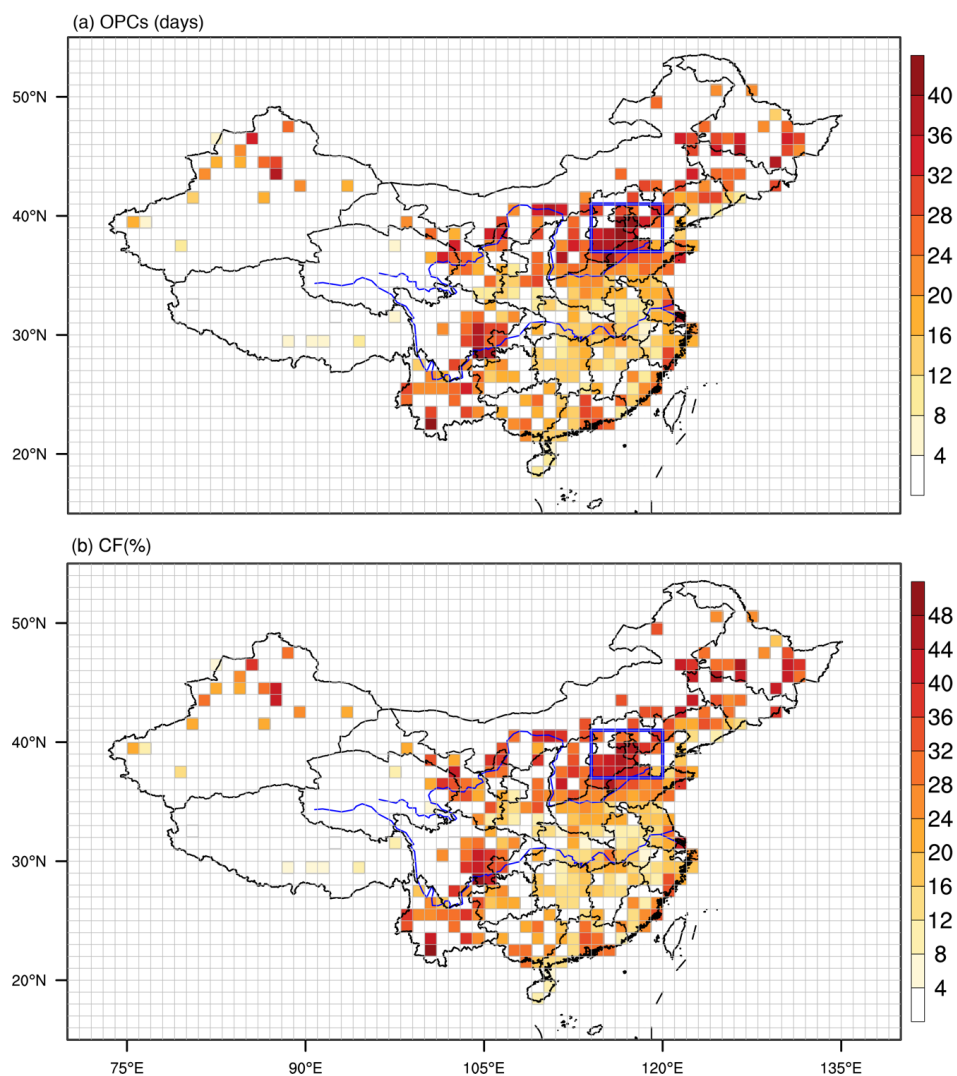
547



548 **Table 1** Simulated net changes in O₃ mass (Gg O₃ d⁻¹) in the boundary layer due to different
549 processes in North China Plain (37–41°N, 114–120°E) during OPCs and OPIs of 2014–2017,
550 as well as their differences (OPCs - OPIs).

	Net chemical production	Horizontal advection	Vertical advection	Diffusion plus dry deposition
OPCs	17.10	-2.65	1.12	-6.95
OPIs	15.66	-1.38	1.24	-7.10
Differences	1.44	-1.27	-0.12	0.15

551



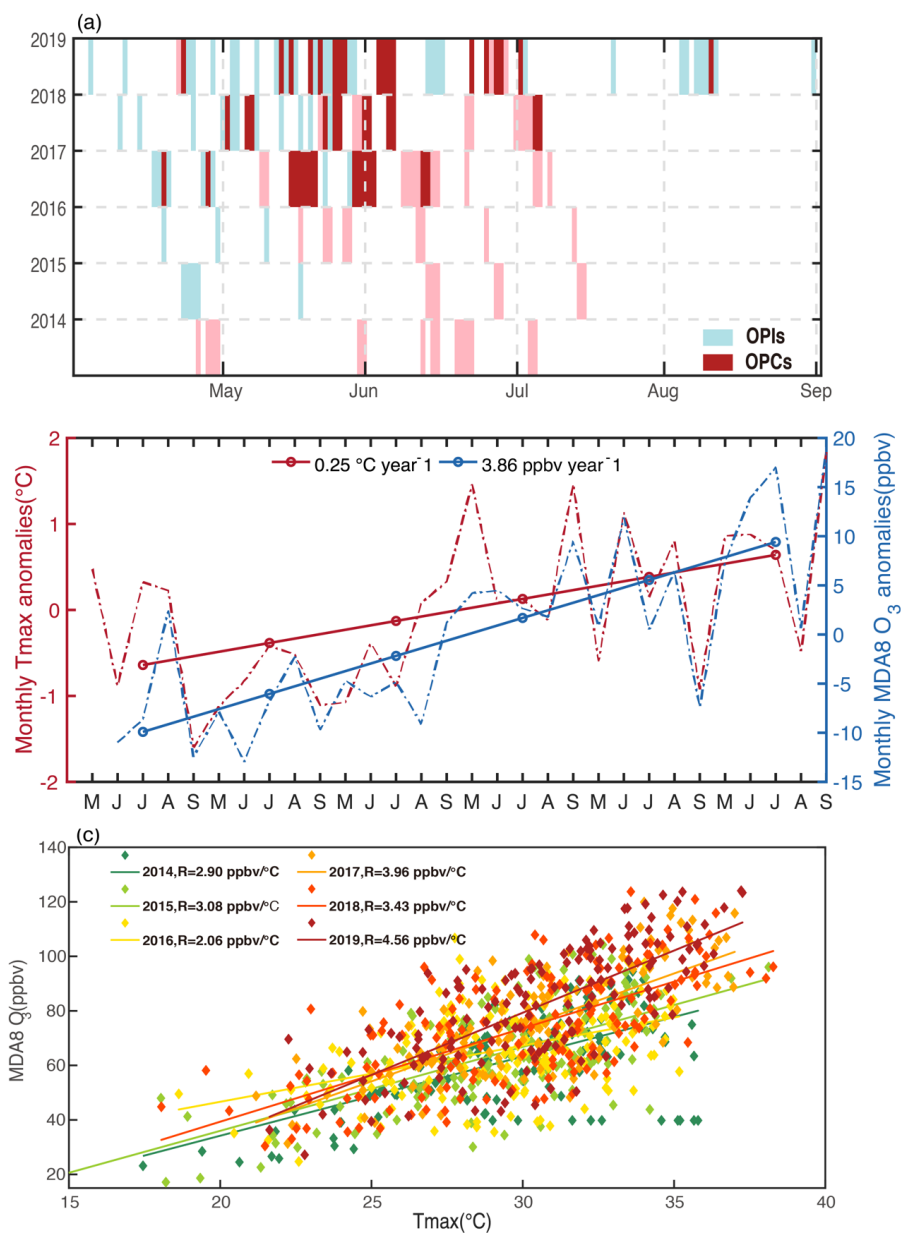
552

553 **Figure 1** Spatial patterns of (a) OPCs (days), frequency of coupled extremes in high temperatures

554 and surface O₃ concentration, and (b) the corresponding CF values (%), ratio of F_{OPC} to total O₃

555 pollution days, during May-September of 2014-2019 from observations. The blue box area indicates

556 the NCP region (37-41°N; 114 -120°E).



557

558 **Figure 2** (a) Observed daily variations of the occurrence of OPIs (blue) and OPCs (red) in NCP

559 during 2014-2019. The pink boxes indicate hot days when daily Tmax exceeds its threshold while

560 MDA8 O₃ does not exceed its threshold. (b) Monthly mean MDA8 O₃ (blue dashed line) and Tmax

561 (magenta dashed line) anomalies during May to September of 2014–2019 for the NCP region. For

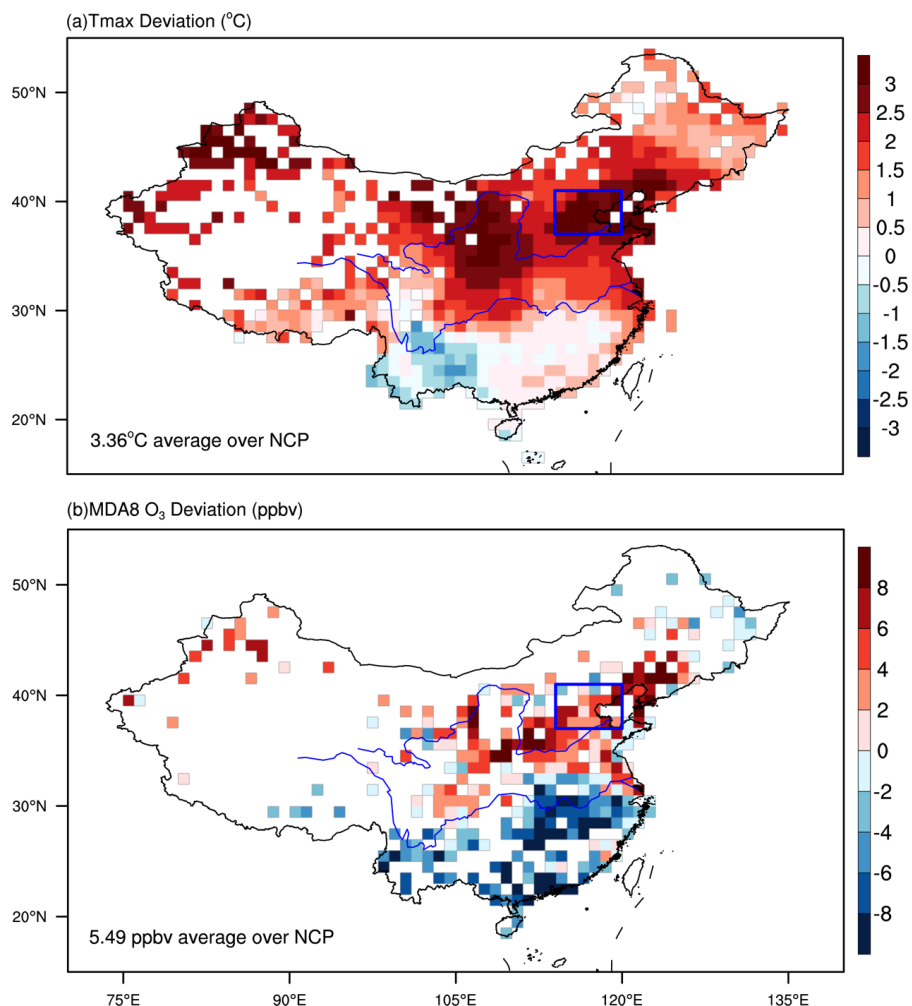


562 each month, anomalies are computed relative to the 2014–2019 means for that month of the year.
563 The linear trends of the 5-month averaged MDA8 O₃ and Tmax anomalies for each year is shown
564 by the solid lines, with the regression slopes shown near the top of the panel. (c) Scatterplot of daily
565 MDA8 O₃ versus Tmax over NCP for May-September of each year identified by the color in 2014-
566 2019. Linear regression lines and the slope (R) values (unit: ppbv/°C) are shown for each year,
567 indicating a general trend of increasing R from 2014 to 2019.

568

569

570



571

572 **Figure 3** Spatial patterns of the averaged difference in (a) Tmax and (b) MDA8 O₃ between OPCs

573 and OPIs (OPCs minus OPIs). The blue box in each panel indicates the NCP region (37-41°N; 114-

574 120°E).

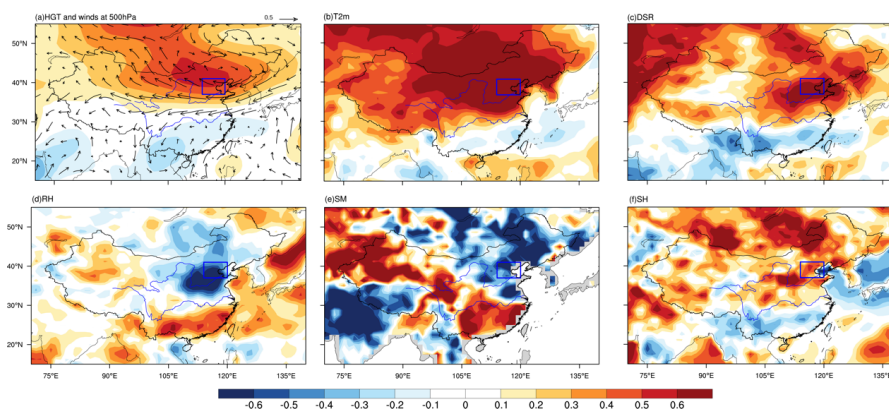
575

576

577



578



579

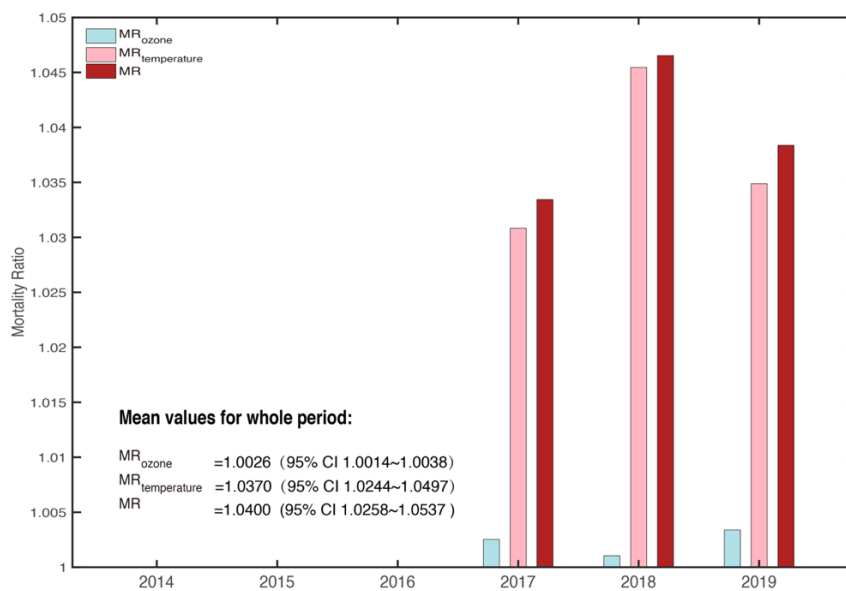
580 **Figure 4** Composites of normalized anomalous (a) geopotential height (HGT) and winds at 500hPa,
581 (b) 2m air temperature (T2m), (c) downward solar radiation flux (DSR), (d) relative humidity (RH),
582 (e) soil moisture content (SM), and (f) sensible heat flux (SH) at the surface during coupled extremes
583 (OPCs). The blue box in each panel indicates the NCP region.

584

585

586

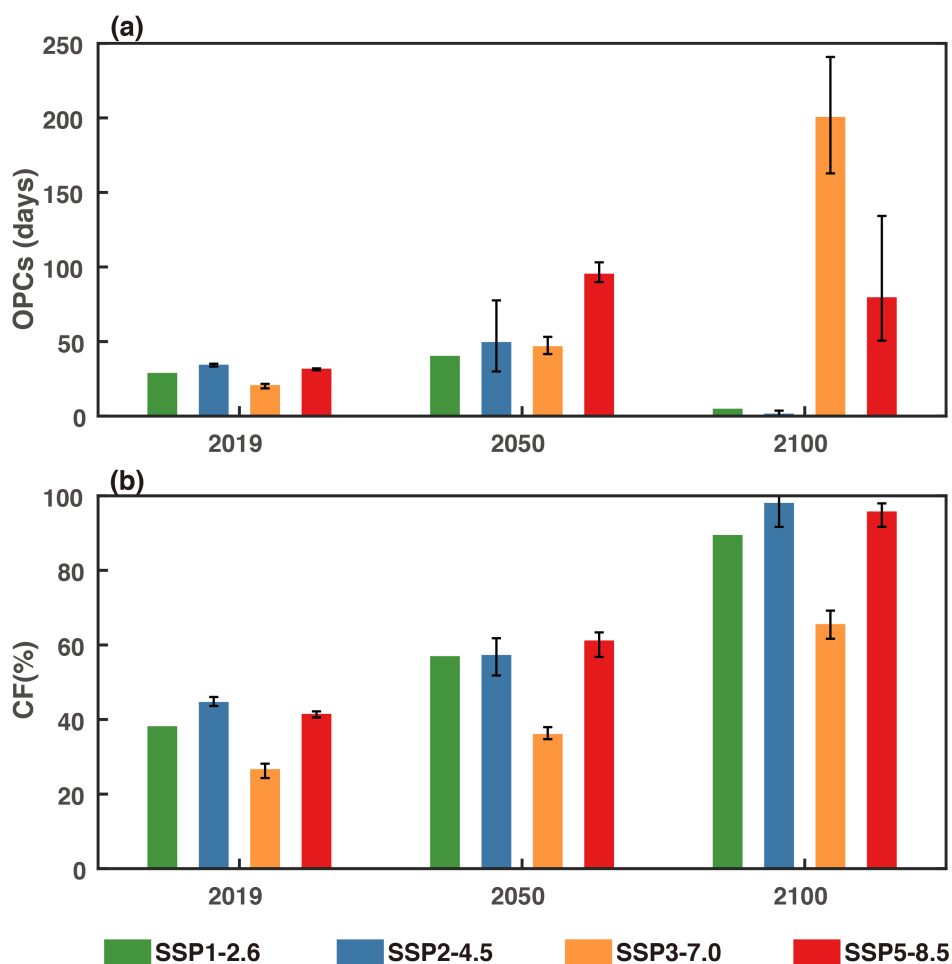
587



588

589 **Figure 5** MR_{ozone}, MR_{temperature} and MR between OPCs and OPCs during May to September for
590 each year of 2017-2019. The average values for 2017-2019 are given in the left corner. MR_{ozone},
591 MR_{temperature} and MR indicate the mortality changes between OPCs and OPIs due to differences
592 in O₃ levels alone, air temperatures alone and both O₃ levels and temperatures, respectively.

593



594

595 **Figure 6** Averaged (a) OPCs and (b) CF values over NCP based on CMIP6 simulations under

596 different SSPs for the periods of 2015-2019, 2046-2050, and 2096-2100. The error bar shows the

597 minimum and maximum values simulated by the CMIP6 models for each SSP. Note that only one

598 GCM is available for SSP1-2.6.

599

600

601